International Journal of Thermophysics, Vol. 23, No. 2, March 2002 (© 2002)

Thermal Behavior of Perfect and Imperfect Contact Composite Slabs Under the Effect of the Hyperbolic Heat Conduction Model

A. F. Khadrawi,[1] M. A. Al-Nimr,[2, 3] and M. Hammad[4]

Received May 23, 2001

This work studies the heat transfer mechanisms during rapid heating of two-layer composite thin slabs from a macroscopic point of view using the hyperbolic heat conduction model. The composite slabs consist of two thin metal layers which may be in perfect or imperfect thermal contact. The effects of parameters such as the two films' thickness ratio, thermal conductivity ratio, heat capacity ratio, thermal relaxation time, and interfacial heat transfer coefficient on the thermal behavior of the composite slabs are investigated.

KEY WORDS: composite slab; conduction; hyperbolic heat conduction; thermal behavior; thermal waves; two-layer slab.

1. INTRODUCTION

In the classical theory of diffusion, the heat flux vector ($\mathbf{q}$) and the temperature gradient (∇T) across a material volume are assumed to occur at the same instant of time. Fourier's law of heat conduction,

$$\mathbf{q}(x, t) = -k\nabla T(x, t) \tag{1}$$

where $\mathbf{q}$ is the heat flux vector, k is the thermal conductivity, and t is the physical time, dictates such an immediate response. It results in an infinite speed of heat propagation, implying that the thermal distribution applied at a certain location in a solid medium can be sensed immediately anywhere

[1] Mechanical Engineering Department, Al-Balqa' Applied University, Al-Salt, Jordan.
[2] Mechanical Engineering Department, Jordan University of Science and Technology, P.O. Box 3030, Irbid 22110, Jordan.
[3] To whom correspondence should be adressed. E-mail: malnimr@just.edu.jo
[4] Mechanical Engineering Department, Jordan University, Amman, Jordan.

0195-928X/02/0300-0581/0 © 2002 Plenum Publishing Corporation

else in the medium. Because the heat flux vector and the temperature gradient are simultaneous, there is no difference between the cause and the effect of heat flow. However, there are applications in which heat is found to propagate at a finite speed. These applications involve very low temperatures, near absolute zero, energy sources such as a laser or a microwave with an extremely short duration or a very high frequency, very high temperature gradient, and extremely short times. A specific example of one of the above applications is the use of short-pulse lasers in the fabrication of microstructures, the synthesis of advanced materials, measurements of thin-film properties, diagnostics of material structure transformation, micomachining, laser patterning, laser processing of diamond films from carbon ion-implanted copper substrates, and laser surface hardening. To account for the phenomena involving the finite propagation velocity of the thermal wave, the classical Fourier heat flux should be modified. Cattaneo [1] and Vernotte [2] suggested independently a modified heat flux model in the form

$$\mathbf{q}(x, t+\tilde{\tau}) = -k \frac{\partial T(x, t)}{\partial x} \tag{2}$$

where $\tilde{\tau}$ is the time delay, called the "relaxation time." The constitutive law of Eq. (2) assumes that the heat flux vector (the effect) and the temperature gradient (the cause) across a material volume occur at different instants in time, and the time delay between the heat flux and the temperature gradient is the relaxation time $\tilde{\tau}$. The first-order expansion of $\mathbf{q}$ in Eq. (2) with respect to t bridges all the physical quantities at the same time. It results in the expansion

$$\tau \frac{\partial \mathbf{q}(x, t)}{\partial t} + \mathbf{q}(x, t+\tilde{\tau}) = -k \frac{\partial T(x, t)}{\partial x} \tag{3}$$

In Eq. (3) it is assumed that $\tilde{\tau}$ is sufficiently small so that the first-order Taylor expansion of $\mathbf{q}(x, t+\tilde{\tau})$ is an accurate representation of the convection heat flux. The equation of energy conservation for such problems is given as

$$\rho c \frac{\partial T}{\partial t} = -\frac{\partial \mathbf{q}}{\partial x} \tag{4}$$

where ρ is the density and c is the specific heat. Elimination of $\mathbf{q}$ between Eq. (3) and Eq. (4) leads to the hyperbolic heat conduction equation,

$$\rho c \tilde{\tau} \frac{\partial^2 T}{\partial t^2} + \rho c \frac{\partial T}{\partial t} = k \frac{\partial^2 T}{\partial x^2} \tag{5}$$

The wave model represented in Eq. (5) removes the paradox of the finite speed of heat propagation assumed in Fourier's law. Tzou [3] relates the relaxation time to the thermal wave speed as

$$\tilde{\tau} = \frac{\alpha}{C^2}$$

where α is the thermal diffusivity and C is the thermal wave speed. In the case of C approaching infinity, the relaxation time decreases to zero ($\tilde{\tau} = 0$) and the wave model reduces to Fourier's law. The Cattaneo [1] and Vernotte [2] (*CV*) wave model assumes an instantaneous heat flow. The temperature gradient is always the cause for the heat transfer, while the heat flux vector is always the effect.

It is worth mentioning here that the relaxation time $\tilde{\tau}$ is of the order of picoseconds. Use of the hyperbolic heat conduction model is essential when the problem time scale, which is the duration of the transient heating process, is comparable with the thermal relaxation time $\tilde{\tau}$.

The hyperbolic heat conduction model as given in Eq. (5) has been receiving increasing attention both for theoretical motivations (e.g., analysis of thermal waves and second sound in dieletric solids and finite speed of heat transport) and for the analysis of some practical problems involving a fast source of thermal energy as mentioned previously.

2. CASE STUDY

Consider a two-layer slab that consists of the first layer for $0 \leqslant x \leqslant a$ and the second layer for $a \leqslant x \leqslant b$, which are in perfect or imperfect thermal contact as illustrated in Fig. 1. Let k_1 and k_2 be the thermal

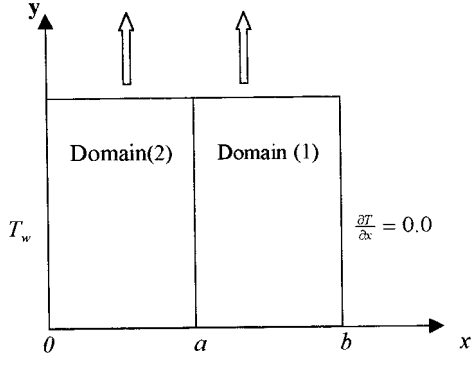

Fig. 1. Schematic diagram of the problem under consideration.

conductivities, and α_1 and α_2 be the thermal diffusivities for the first and second layers, respectively. Knowledge of transient heat conduction in a two-layer composite thin slab is of importance in a number of applications such as in coating, cladding, foil formation, fabrication of p–n junctions, and semiconductors and electronic chips. Initially, the first and second regions are at temperature T_i. For $t > 0$ the boundary surface at $x = 0$ is kept at T_w and the boundary surface at $x = b$ is kept insulated. The thickness of the two layers is assumed to be very small relative to the height of the slab, so it is reasonable to assume that the conducted heat is transferred in the x-direction only.

The elementary assumption here is that the heat propagates with a finite speed. Thus, the hyperbolic heat conduction model is suitable for accounting for the phenomena concerning the finite propagation speed of the thermal wave.

2.1. Perfect Contact

In this case, the energy equations coupled at the interface have to be solved. These equations are written

$$\rho_1 c_1 \frac{\partial T_1(x, t)}{\partial t} = -\frac{\partial q_1}{\partial x} \tag{6}$$

$$\rho_2 c_2 \frac{\partial T_2(x, t)}{\partial t} = -\frac{\partial q_2}{\partial x} \tag{7}$$

$$q_1 + \tilde{\tau}_{q,1} \frac{\partial q_1}{\partial t} = -k_1 \frac{\partial T_1}{\partial x} \tag{8}$$

$$q_2 + \tilde{\tau}_{q,2} \frac{\partial q_2}{\partial t} = -k_2 \frac{\partial T_2}{\partial x} \tag{9}$$

Combine Eqs. (6) and (8), and Eqs. (7) and (9), to yield

$$\tilde{\tau}_{q,1} \frac{\partial^2 T_1(x, t)}{\partial t^2} + \frac{\partial T_1(x, t)}{\partial t} = \alpha_1 \frac{\partial^2 T_1(x, t)}{\partial x^2} \qquad \text{for} \quad 0 \leqslant x \leqslant a \tag{10}$$

$$\tilde{\tau}_{q,2} \frac{\partial^2 T_2(x, t)}{\partial t^2} + \frac{\partial T_2(x, t)}{\partial t} = \alpha_2 \frac{\partial^2 T_2(x, t)}{\partial x^2} \qquad \text{for} \quad a \leqslant x \leqslant b \tag{11}$$

which assume that K_1, K_2 are not functions of the coordinates or of T_1, T_2, respectively, and that the following initial and boundary conditions hold:

$$T_1(x, 0) = T_2(x, 0) = T_i$$

$$\frac{\partial T_1(x, 0)}{\partial t} = \frac{\partial T_1(x, 0)}{\partial t} = 0.0$$

$$T_1(0, t) = T_w$$

$$\frac{\partial T_2(b, t)}{\partial x} = 0$$

$$T_1(a, t) = T_2(a, t)$$

$$q_1(a, t) = q_2(a, t)$$

Using the following dimensionless parameters,

$$\theta = \frac{T - T_w}{T_i - T_w}, \qquad \xi = \frac{x}{a}, \qquad \eta = \frac{\alpha_1 t}{a^2}, \qquad \tau = \frac{\tilde{\tau}\alpha_1}{a^2}, \qquad Q = \frac{qa}{k_1 \Delta T}$$

Equations (6) to (11) and their initial and boundary conditions become

$$\frac{\partial \theta_1}{\partial \eta} = -\frac{\partial Q_1}{\partial \xi} \tag{12}$$

$$\frac{\partial \theta_2}{\partial \eta} = -\frac{1}{C_R}\frac{\partial Q_2}{\partial \xi} \tag{13}$$

$$Q_1 + \tau_{q,1}\frac{\partial Q_1}{\partial \eta} = -\frac{\partial \theta_1}{\partial \xi} \tag{14}$$

$$Q_2 + \tau_{q,2}\frac{\partial Q_2}{\partial \eta} = -K_r\frac{\partial \theta_2}{\partial \xi} \tag{15}$$

$$\tau_{q,1}\frac{\partial^2 \theta_1}{\partial \eta^2} + \frac{\partial \theta_1}{\partial \eta} = \frac{\partial^2 \theta_1}{\partial \xi^2}, \qquad 0 \leqslant \xi \leqslant 1.0 \tag{16}$$

$$\tau_{q,2}\frac{\partial^2 \theta_2}{\partial \eta^2} + \frac{\partial \theta_2}{\partial \eta} = \alpha_r\frac{\partial^2 \theta_2}{\partial \xi^2}, \qquad 1.0 \leqslant \xi \leqslant R \tag{17}$$

$$\begin{aligned} \theta_1(\xi, 0) &= \theta_2(\xi, 0) = 1.0 \\ \frac{\partial \theta_1(\xi, 0)}{\partial \eta} &= \frac{\partial \theta_2(\xi, 0)}{\partial \eta} = 0.0 \end{aligned} \tag{18}$$

$$\begin{aligned} \theta_1(0,\eta) &= 0.0 \\ \frac{\partial\theta_2(R,\eta)}{\partial\xi} &= 0.0 \\ \theta(1,\eta_1) &= \theta_2(1,\eta) \\ Q_1(1,\eta) &= Q_2(1,\eta) \end{aligned} \tag{19}$$

where $K_r = k_2/k_1$ is the thermal conductivity ratio, $\alpha_r = \alpha_2/\alpha_1$ is the thermal diffiusivity ratio, and $R = b/a$. From the definition of R, it is clear that $(R-1)$ represents the dimensionless thickness $(=\frac{(b-a)}{a})$ of domain 2.

Now, with the notation that $L\{\theta(\xi,\eta)\} = W(\xi, S)$, Laplace transformations of Eqs. (16) and (17) yield

$$\frac{d^2W_1}{d\xi^2} - (\tau_{q,1}S^2 + S)\,W_1 = -(1+\tau_{q,1}S) \tag{20}$$

$$\frac{d^2W_2}{d\xi^2} - \left(\frac{\tau_{q,2}S^2+S}{\alpha_r}\right)W_2 = -\left(\frac{\tau_{q,2}S+1}{\alpha_r}\right) \tag{21}$$

These two equations assume the following solutions:

$$W_1(\xi, S) = C_1 e^{M_1\xi} + C_2 e^{-M_1\xi} + \frac{1}{S} \tag{22}$$

$$W_2(\xi, S) = C_3 e^{M_2\xi} + C_4 e^{-M_2\xi} + \frac{1}{S} \tag{23}$$

where $M_1 = \sqrt{(\tau_{q,1}S^2+S)}$ and $M_2 = \sqrt{(\tau_{q,2}S^2+S)/\alpha_r}$.

Also, with the notation that $V = L\{Q\}$, the Laplace transform of Eq. (19) yields

$$\begin{aligned} W_1(0,S) &= 0 \\ \frac{\partial W_2(R,S)}{\partial\xi} &= 0 \\ W_1(1,S) &= W_2(1,S) \\ V_1(1,S) &= V_2(1,S) \end{aligned} \tag{24}$$

From Eqs. (14) and (15) with $Q_1(\xi,0) = Q_2(\xi,0) = 0$, we have

$$\frac{dW_1(1,S)}{d\xi} = \left(\frac{K_r(1+\tau_{q,1}S)}{(1+\tau_{q,2}S)}\right)\frac{dW_2(1,S)}{d\xi}$$

Insert Eqs. (22) and (23) into (24) and solve for C_1, C_2, C_3, and C_4 to yield

$$C_1 = \frac{\left(-\frac{1}{S}\right)\left\{\frac{e^{-2M_1}\left[\left(1+\frac{K_r}{\sqrt{\alpha_r}}\sqrt{\frac{(1+\tau_{q,1}S)}{(1+\tau_{q,2}S)}}\right)+\left(1-\frac{K_r}{\sqrt{\alpha_r}}\sqrt{\frac{(1+\tau_{q,1}S)}{(1+\tau_{q,2}S)}}\right)(e^{M_2(2R-2)})\right]}{\left[\left(1-\frac{K_r}{\sqrt{\alpha_r}}\sqrt{\frac{(1+\tau_{q,1}S)}{(1+\tau_{q,2}S)}}\right)+\left(1-\frac{K_r}{\sqrt{\alpha_r}}\sqrt{\frac{(1+\tau_{q,1}S)}{(1+\tau_{q,2}S)}}\right)(e^{M_2(2R-2)})\right]}\right\}}{\left\{1+\frac{e^{-2M_1}\left[\left(1+\frac{K_r}{\sqrt{\alpha_r}}\sqrt{\frac{(1+\tau_{q,1}S)}{(1+\tau_{q,2}S)}}\right)+\left(1-\frac{K_r}{\sqrt{\alpha_r}}\sqrt{\frac{(1+\tau_{q,1}S)}{(1+\tau_{q,2}S)}}\right)(e^{M_2(2R-2)})\right]}{\left[\left(1-\frac{K_r}{\sqrt{\alpha_r}}\sqrt{\frac{(1+\tau_{q,1}S)}{(1+\tau_{q,2}S)}}\right)+\left(1-\frac{K_r}{\sqrt{\alpha_r}}\sqrt{\frac{(1+\tau_{q,1}S)}{(1+\tau_{q,2}S)}}\right)(e^{M_2(2R-2)})\right]}\right\}}$$

$$C_2 = \frac{-1/S}{\left\{1+\frac{e^{-2M_1}\left[\left(1+\frac{K_r}{\sqrt{\alpha_r}}\sqrt{\frac{(1+\tau_{q,1}S)}{(1+\tau_{q,2}S)}}\right)+\left(1-\frac{K_r}{\sqrt{\alpha_r}}\sqrt{\frac{(1+\tau_{q,1}S)}{(1+\tau_{q,2}S)}}\right)(e^{M_2(2R-2)})\right]}{\left[\left(1+\frac{K_r}{\sqrt{\alpha_r}}\sqrt{\frac{(1+\tau_{q,1}S)}{(1+\tau_{q,2}S)}}\right)+\left(1-\frac{K_r}{\sqrt{\alpha_r}}\sqrt{\frac{(1+\tau_{q,1}S)}{(1+\tau_{q,2}S)}}\right)(e^{M_2(2R-2)})\right]}\right\}}$$

$$C_3 = \frac{C_1 e^{M_1} + C_2 e^{M_1}}{e^{M_2}(1+e^{M_2(2R-2)})} \qquad \text{and} \qquad C_4 = \left\{\frac{C_1 e^{M_1} + C_2 e^{M_1}}{e^{M_2}(1+e^{M_2(2R-2)})}\right\} e^{2RM_2}$$

Equations (22) and (23) are inverted using a computer program based on the Riemannsum approximation as

$$\theta_k(\xi,\eta) \cong \frac{e^{\gamma\eta}}{\eta}\left[\frac{1}{2}W_k(\xi,\gamma) + \mathrm{Re}\sum_{n=1}^{N} W_k\left(\xi, \gamma+\frac{in\pi}{\eta}\right)(-1)^n\right] \tag{25}$$

where $k=1$ for domain 1 and $k=2$ for domain 2. In Eq. (25), Re represents the real part of the summation and $i=\sqrt{-1}$, and $\gamma\eta = 4.7$ gives the most satisfactory results [3]. Equation (25) yields the exact temperature distribution numerically in both domains for the perfect contact case.

2.2. Imperfect Contact

In a manner similar to what has been done for the perfect contact case, the energy equations coupled at the interface have to be solved with different boundary conditions. In the case of perfect contact, the temperatures at the interface are equal, while in this case the temperatures at the interface are related as

$$q_1(1,\eta) = h[T_1(1,\eta) - T_2(1,\eta)]$$

where h is the interfacial convective heat transfer coefficient. The energy equations in dimensionless form are given as

$$\frac{\partial \theta_1}{\partial \eta} = -\frac{\partial Q_1}{\partial \xi} \tag{26}$$

$$\frac{\partial \theta_2}{\partial \eta} = -\frac{1}{C_R}\frac{\partial Q_2}{\partial \xi} \tag{27}$$

$$Q_1 + \tau_{q,1}\frac{\partial Q_1}{\partial \eta} = -\frac{\partial \theta_1}{\partial \xi} \tag{28}$$

$$Q_2 + \tau_{q,2}\frac{\partial Q_2}{\partial \eta} = -K_r\frac{\partial \theta_2}{\partial \xi} \tag{29}$$

Combining Eqs. (26) and (28), and Eqs. (27) and (29), yields

$$\tau_{q,1}\frac{\partial^2 \theta_1}{\partial \eta^2} + \frac{\partial \theta_1}{\partial \eta} = \frac{\partial^2 \theta_1}{\partial \xi^2}, \qquad 0 \leqslant \xi \leqslant 1.0 \tag{30}$$

$$\tau_{q,2}\frac{\partial^2 \theta_2}{\partial \eta^2} + \frac{\partial \theta_2}{\partial \eta} = \alpha_r\frac{\partial^2 \theta_2}{\partial \xi^2}, \qquad 1.0 \leqslant \xi \leqslant R \tag{31}$$

Subject to the following initial and boundary conditions,

$$\theta_1(\xi, 0) = \theta_2(\xi, 0) = 1$$
$$\frac{\partial \theta_1(\xi, 0)}{\partial \eta} = \frac{\partial \theta_2(\xi, 0)}{\partial \eta} = 0 \tag{32}$$

$$\theta_1(0, \eta) = 0$$
$$\frac{\partial \theta_2(R, \eta)}{\partial \xi} = 0$$
$$Q_1(1, \eta) = Q_2(1, \eta) \tag{33}$$
$$Q_1(1, \eta) = \mathrm{Bi}(\theta_1(1, \eta) - \theta_2(1, \eta))$$

where $K_r = k_2/k_1$ is the thermal conductivity ratio, $\alpha_r = \alpha_2/\alpha_1$ is the thermal diffiusivity ratio, $R = b/a$, and Bi is the $Biot$ number, which is defined as ha/k_1.

Now, with the notation that $L\{\theta(\xi, \eta)\} = W(\xi, S)$, the Laplace transforms of Eqs. (30) and (31) yield

$$\frac{d^2W_1}{d\xi^2} - (\tau_{q,1}S^2 + S)\,W_1 = -(1 + \tau_{q,1}S) \tag{34}$$

$$\frac{d^2W_2}{d\xi^2} - \left(\frac{\tau_{q,2}S^2 + S}{\alpha_r}\right)W_2 = -\left(\frac{\tau_{q,2}S + 1}{\alpha_r}\right) \tag{35}$$

These two equations assume the following solutions:

$$W_1(\xi, S) = C_1 e^{M_1\xi} + C_2 e^{-M_1\xi} + \frac{1}{S} \tag{36}$$

$$W_2(\xi, S) = C_3 e^{M_2\xi} + C_4 e^{-M_2\xi} + \frac{1}{S} \tag{37}$$

where $M_1 = \sqrt{(\tau_{q,1}S^2 + S)}$ and $M_2 = \sqrt{(\tau_{q,2}S^2 + S)/\alpha_r}$.

Also, with the notation that $V = L\{Q\}$, the Laplace transform of Eq. (33) yields

$$W_1(0, S) = 0 \tag{38a}$$

$$\frac{dW_2(R, S)}{\partial\xi} = 0 \tag{38b}$$

$$V_1(1, S) = V_2(1, S)$$

From Eqs. (28) and (29) with $Q_1(\xi, 0) = Q_2(\xi, 0) = 0$ and $V_1(1, S) = V_2(1, S)$, we obtain

$$\frac{dW_1(1, S)}{d\xi} = \left(\frac{K_r(1 + \tau_{q,1}S)}{(1 + \tau_{q,2}S)}\right)\frac{dW_2(1, S)}{d\xi} \tag{38c}$$

Also, the interfacial boundary condition becomes

$$\frac{dW_1(1, S)}{d\xi} = -\mathrm{Bi}(1 + \tau_{q,1}S)[W_1(1, S) - W_2(1, S)] \tag{38d}$$

Insert Eqs. (36) and (37) into Eqs. (38a) to (38d) and solve for C_1, C_2, C_3, and C_4 to yield

$$C_1 = \frac{\left(-\frac{1}{S}\right)\left\{\dfrac{e^{-2M_1}\left[\beta(1+e^{M_2(2R-2)})+\dfrac{K_r(M_1-\beta)}{\sqrt{\alpha_r}}\sqrt{\dfrac{(1+\tau_{q,1}S)}{(1+\tau_{q,2}S)}}(e^{M_2(2R-2)}-1)\right]}{\left[\dfrac{K_r(M_1-\beta)}{\sqrt{\alpha_r}}\sqrt{\dfrac{(1+\tau_{q,1}S)}{(1+\tau_{q,2}S)}}(e^{M_2(2R-2)}-1)+\beta(1+e^{M_2(2R-2)})\right]}\right\}}{\left\{1+\dfrac{e^{-2M_1}\left[\beta(1+e^{M_2(2R-2)})+\dfrac{K_r(M_1-\beta)}{\sqrt{\alpha_r}}\sqrt{\dfrac{(1+\tau_{q,1}S)}{(1+\tau_{q,2}S)}}(e^{M_2(2R-2)}-1)\right]}{\left[\dfrac{K_r(M_1-\beta)}{\sqrt{\alpha_r}}\sqrt{\dfrac{(1+\tau_{q,1}S)}{(1+\tau_{q,2}S)}}(e^{M_2(2R-2)}-1)+\beta(1+e^{M_2(2R-2)})\right]}\right\}}$$

$$C_2 = \frac{-\frac{1}{S}}{\left\{1+\dfrac{e^{-2M_1}\left[\beta(1+e^{M_2(2R-2)})+\dfrac{K_r(M_1-\beta)}{\sqrt{\alpha_r}}\sqrt{\dfrac{(1+\tau_{q,1}S)}{(1+\tau_{q,2}S)}}(e^{M_2(2R-2)}-1)\right]}{\left[\dfrac{K_r(M_1-\beta)}{\sqrt{\alpha_r}}\sqrt{\dfrac{(1+\tau_{q,1}S)}{(1+\tau_{q,2}S)}}(e^{M_2(2R-2)}-1)+\beta(1+e^{M_2(2R-2)})\right]}\right\}}$$

$$C_3 = \frac{C_1(M_1+\beta)\,e^{-M_1} - C_2(M_1-\beta)\,e^{-M_1}}{\beta e^{-M_1}(1+e^{M_2(2R-2)})}$$

$$C_4 = \left\{\frac{C_1(M_1+\beta)\,e^{-M_1} - C_2(M_1-\beta)\,e^{-M_1}}{\beta e^{-M_1}(1+e^{M_2(2R-2)})}\right\} e^{2RM_2}$$

Equations (36) and (37) are inverted using a computer program based on the Riemannsum approximation as

$$\theta_k(\xi,\eta) \cong \frac{e^{\gamma\eta}}{\eta}\left[\frac{1}{2}W_k(\xi,\gamma) + \mathrm{Re}\sum_{n=1}^{N} W_k\left(\xi, \gamma+\frac{in\pi}{\eta}\right)(-1)^n\right] \tag{39}$$

where $k=1$ for domain (1) and $k=2$ for domain (2). In Eq. (39), Re represents the real part of the summation and $i=\sqrt{-1}$, and $\gamma\eta = 4.7$ gives the most satisfactory results [3]. Equation (39) yields the exact temperature distribution in both domains for imperfect contact case.

3. RESULTS AND DISCUSSION

Figures 2 to 4 show the effect of the interfacial Biot number on the spatial temperature distribution within the two domains. It is clear from Figs. 2 and 3 that the temperature distribution for the imperfect contact case approaches that for the perfect contact case as Bi increases. Also, the

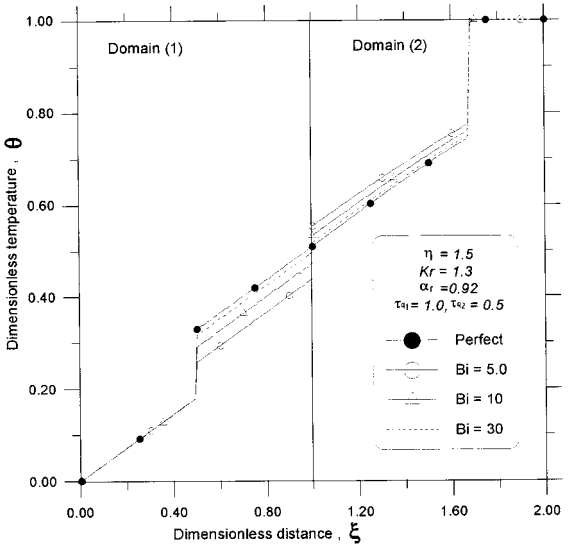

Fig. 2. Spatial temperature distribution within the two domains for perfect and imperfect contact using the hyperbolic heat conduction model.

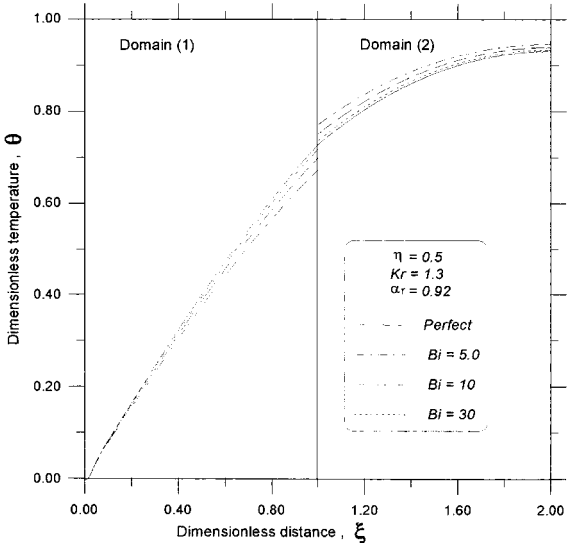

Fig. 3. Spatial temperature distribution within the two domains for perfect and imperfect contact using the parabolic heat conduction model.

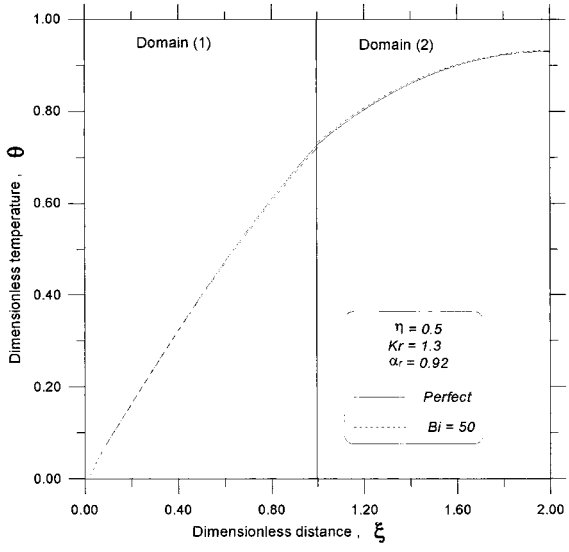

Fig. 4. Spatial temperature distribution within the two domains for perfect and imperfect contact using the parabolic heat conduction model.

interfacial temperature jump decreases as the Bi number increases. Using the thermal perfect contact assumption, the temperature is overestimated in the first domain, which is adjacent to the heat transfer boundary, i.e., the boundary at which the cooling effect is applied. On the other hand, the perfect thermal contact assumption underestimates the temperature within the second domain adjacent to the insulated boundary. The appearance of the discontinuity in the temperature profile in Fig. 2 at $\xi = 0.5$ and $\xi = 1.7$ is due to the wave nature of the hyperbolic heat conduction model. As mentioned previously, the hyperbolic heat conduction model assumes that heat propagates at a finite speed in the form of a wave. The appearance of these discontinuities depends on the specific location within the slab, on time, and other thermal properties of the two layers especially on the thermal relaxation times τ_{q1} and τ_{q2}. For large thermal relaxation times τ_{q1} and τ_{q2} the appearance of these discontinuities is very likely. This is the reason why, for example, these discontinuities do not appear in Fig. 6 which assumes very small values of τ_{q1} and τ_{q2}.

Figure 4 shows that an interfacial Biot number larger than 50 yields predictions similar to that of the perfect contact model. Figure 5 shows deviations between the predictions of both perfect and imperfect contact models at different interfacial Biot numbers. In this Fig. 5 Δ is defined as the difference between the dimensionless temperatures obtained under the

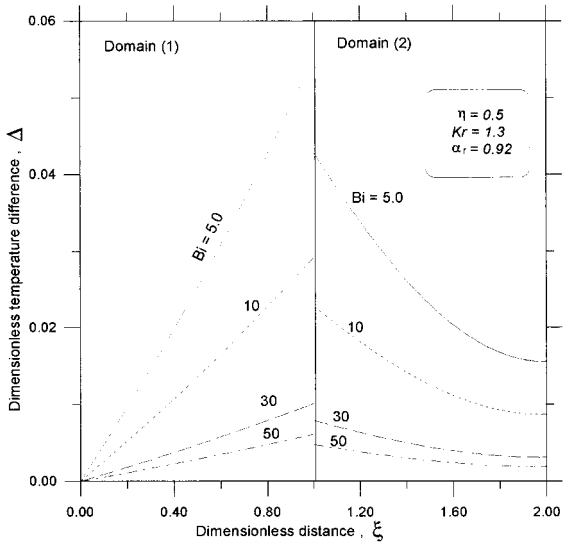

Fig. 5. Effect of Biot number on the temperature distribution difference within the two domains for perfect and imperfect contact using the parabolic heat conduction model.

assumption of perfect contact and imperfect contact. It is clear that the deviation decreases as Bi increases. The deviation in the domain adjacent to the cooling boundary is larger than that in the domain adjacent to the insulated boundary. Also, the deviation has its maximum value at the contact plane. As a result, it is concluded that the deviation between both the perfect and the imperfect contact models is significant very near the contact plane and in locations having high heat transfer rates. Figure 6 shows the spatial temperature distribution using the perfect contact model at different thermal relaxation time τ_q. It is clear from this figure that for τ_q less than 0.01, the thermal relaxation time has insignificant effect on the prediction of the diffusion parabolic model, which assumes that $\tau_{q1} = \tau_{q2} = 0$.

Figure 7 shows the effect of the interfacial Biot number on the transient temperature variation within the two domains. It is clear from this figure that the transient temperature variation for the imperfect contact case approaches that for the perfect contact case as Bi increases. Also, this figure shows that an interfacial Biot number larger than 50 yields predictions similar to that of the perfect contact model. Figure 8 shows the effect of the second domain thickness $(R-1)$ on the predictions of the perfect and imperfect contact models within the first domain. It is clear that the

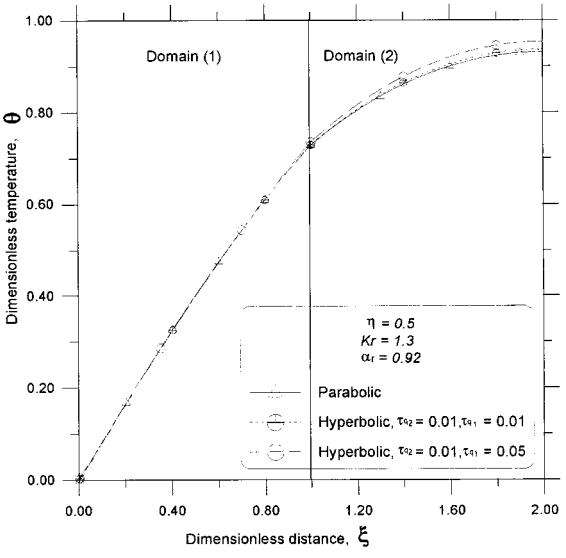

Fig. 6. Spatial temperature distribution within the two domains using the parabolic and the hyperbolic heat conduction models.

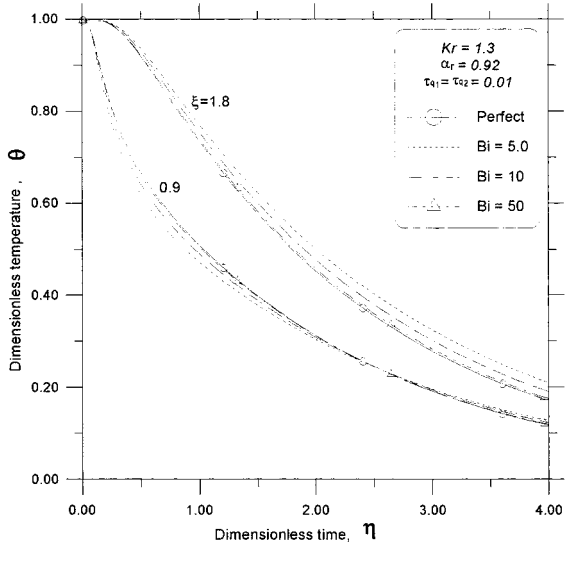

Fig. 7. Transient temperature variation within the two domains for perfect and imperfect contact using the hyperbolic heat conduction model.

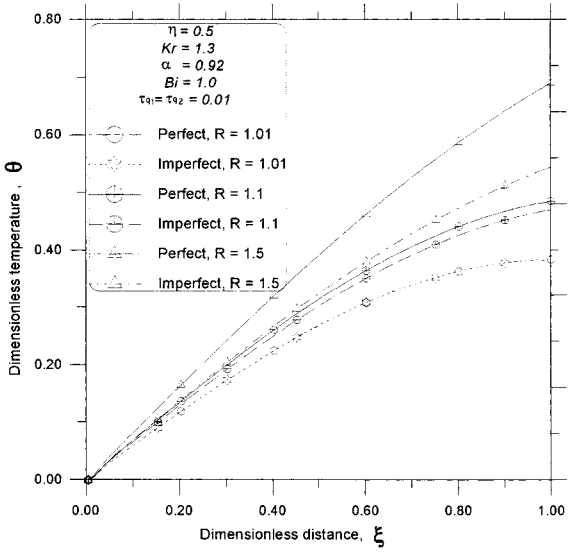

Fig. 8. Spatial temperature distribution within the two domains for perfect and imperfect contact using the hyperbolic heat conduction model at different R.

deviation between both models decreases as the second domain thickness decreases. As the thickness of the second domain decreases, its thermal capacity and thermal resistance decrease and, as a result, the first domain is not affected by the presence of the second domain or by the type of the interfacial thermal conditions at the interface between both domains. For situations involving very thin second domain, the perfect thermal contact assumption is justified.

Figure 9 shows the effect of the thermal conductivity ratio K_r on the predictions of both models within the two domains. It is clear that as K_r increases, the deviation between the predictions of both models decreases in the second domain, which has the higher conductivity, and increases in the first domain, which has the lower conductivity. Domains having a high thermal conductivity are less sensitive to the type of the interfacial thermal conditions. Also, it is clear that the temperature distribution in the domain, which has a higher conductivity, may be assumed spatially lumped. Figure 10 shows the effect of the thermal diffusivity ratio α_r on the deviation between the predictions of both models within the two domains. It is clear that as α_r increases the deviation increases in the second domain and decreases in the first domain. An increase in α_r with a fixed value of K_r implies that the thermal capacity ratio $\{\rho_1 c_1/(\rho_2 c_2)$ increases. The thermal capacity ratio $\rho_1 c_1/(\rho_2 c_2)$ increases by increasing $\rho_1 c_1$ or decreasing $\rho_2 c_2$. As the thermal

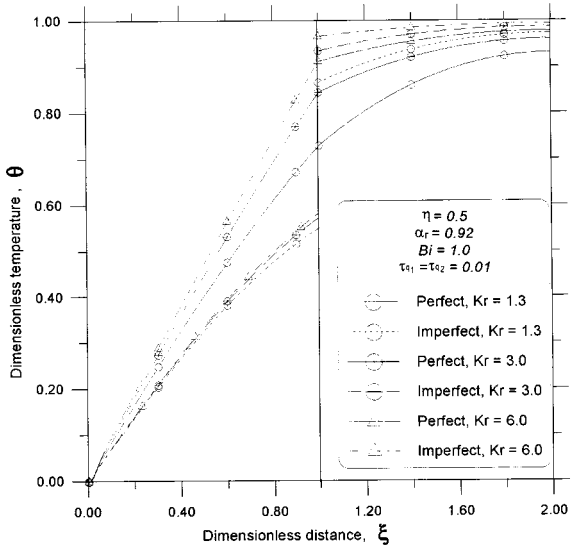

Fig. 9. Spatial temperature distribution within the two domains for perfect and imperfect contact using the hyperbolic heat conduction model at different K_r.

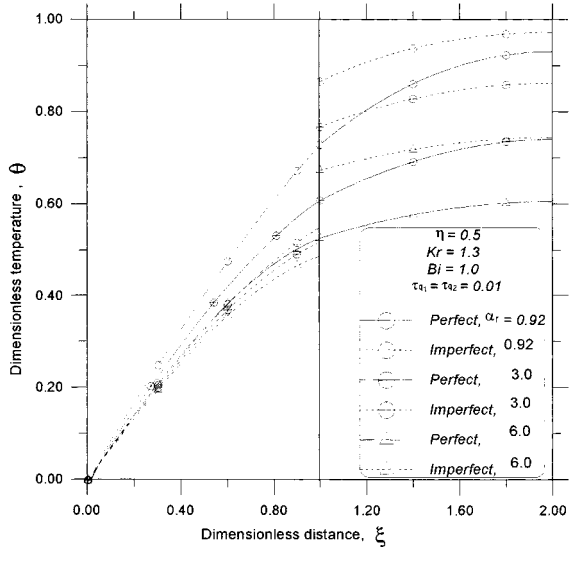

Fig. 10. Spatial temperature distribution within the two domains for perfect and imperfect contact using the hyperbolic heat conduction model at different α_r.

capacity of the first domain increases, then the type of interfacial thermal boundary condition does not cause a significant change in the temperature distribution of the first domain. On the other hand, as $\rho_2 c_2$ decreases, then the type of the interfacial thermal boundary condition causes a significant change in the temperature distribution of the second domain. The temperature distribution within low-thermal capacity domains is very sensitive to any change in the interfacial thermal boundary conditions.

4. CONCLUSIONS

The thermal behavior of a two-layer composite slab under the effect of the hyperbolic heat conduction model is investigated. The layers in the composite slab are in imperfect thermal contact. It is found that the perfect contact model may replace the imperfect contact model for an interfacial *Biot* number larger than 50. The layer adjacent to the heat transfer boundary is more sensitive to the interfacial thermal boundary condition. Also, it is found that the deviation between the predictions of the perfect and the imperfect contact models is more significant in the domain adjacent to the heat transfer boundary and the deviation has its maximum value at the contact plane. The classical heat diffusion model can replace the hyperbolic model when the dimensionless thermal relaxation time of both domains is less than 0.01. The second domain has insignificant effect on the thermal behavior of the first domain when the dimensionless thickness of the second domain is less than 0.1. Also, it is found that the deviation between the perfect and the imperfect contact models is more significant in the domain that has the lower thermal conductivity and the higher thermal diffusivity.

NOMENCLATURE

a	Width of domain 1, m
Bi	Biot number, ha/k_1
c	Specific heat capacity, $J \cdot kg^{-1} \cdot K^{-1}$
f	Specified surface temperature, K
h	Interfacial heat transfer coefficient, $W \cdot m^{-2} \cdot K^{-1}$
k	Thermal conductivity, $W \cdot m^{-1} \cdot K^{-1}$
K_r	Thermal conductivity ratio, k_2/k_1
R	Dimensionless thickness of domain (1 and 2), b/a
t	Time, s
T_1	Temperature of domain 1, K
T_2	Temperature of domain 2, K
T_i	Initial temperature of domain (1 and 2), K

T_∞ Ambient temperature, K
T_w Wall temperature, K
W Laplace transform of the dimensionless temperature
x x-coordinate
y y-coordinate

Greek Symbols

α_r Thermal diffusivity ratio, α_2/α_1
Δ Dimensionless temperature difference between perfect and imperfect thermal contact
η Dimensionless time, $\alpha_1 t/a^2$
θ Dimensionless temperature defined in different forms
ξ Dimensionless x-coordinate, $\frac{x}{a}$
ρ Density, $\mathrm{kg \cdot m^{-3}}$
$\tilde{\tau}$ Thermal relaxation time, s
τ Dimensionless thermal relaxation time, $\frac{\tilde{\tau}\alpha_1}{a^2}$

Subscripts

1 Refers to domain 1
2 Refers to domain 2

REFERENCES

1. C. Catteneo, *Comptes Rendus* **247**:431 (1958).
2. D. Y. Tzou, *Macro- to Microscale Heat Transfer—The Lagging Behavior* (Taylor and Francis, Washington, DC, 1997), pp. 1–64.
3. P. Vernotte, *Comptes Rendus* **252**:2190 (1961).